The Bioscan
AN INTERNATIONAL QUARTERLY JOURNAL OF LIFE SCIENCES
20(4): 2168-2193, 2025 www.thebioscan.com

Design, Synthesis and Antimicrobial Evaluation of Novel Pyridyl-Linked Triazolo[1,5-a]pyrimidine-6-Carboxamide Derivatives

Daizy Chouhan, Neelesh Maheshwari

School of Pharmacy, Sangam University, Bhilwara, Rajasthan, India

DOI: 10.63001/tbs.2025.v20.i04.pp2168-2193

Keywords
Triazolo[1,5-a]pyrimidine; Pyridyl derivatives; Antimicrobial activity; ADME prediction; Molecular docking; Drug-likeness

Received on:

18-10-2025

Accepted on:

21-11-2025

Published on:

30-12-2025

ABSTRACT

The increasing prevalence of antimicrobial resistance necessitates the development of new chemotherapeutic agents with improved efficacy and pharmacokinetic profiles. In the present study, a novel series of pyridyl-linked triazolo[1,5-a] pyrimidine-6-carboxamide derivatives (8a–8h) was rationally designed and synthesized through a multistep synthetic approach. The structures of the synthesized compounds were confirmed by melting point analysis, TLC, ^{1}H NMR, LC-MS, and elemental analysis. All compounds were evaluated for their *in vitro* antimicrobial activity against selected Gram-positive and Gram-negative bacterial strains as well as fungal pathogens using the cup plate diffusion method. Several derivatives exhibited moderate to good antimicrobial activity, with compounds 8d and 8g showing the most promising broad-spectrum effects. *In silico* ADME studies using SwissADME indicated favorable drug-likeness, high predicted gastrointestinal absorption, and full compliance with Lipinski's rule-of-five. Furthermore, molecular docking studies against the bacterial target protein (PDB ID: 1KZN) revealed strong binding affinities and key interactions consistent with the observed biological activity. Collectively, these results suggest that pyridyl-linked triazolo[1,5-a]pyrimidine carboxamides represent a valuable scaffold for further optimization toward the development of novel antimicrobial agents.

Introduction:

The persistent evolution of drug-resistant microbial strains has become a significant worldwide health issue, requiring the discovery and development of innovative antimicrobial medicines with enhanced efficacy, selectivity, and safety profiles [1]. Traditional antibiotics are progressively diminishing in efficacy due to resistance mechanisms include target mutation, enzymatic degradation, and decreased membrane permeability [2]. As a result, medicinal chemistry research has increasingly concentrated on the development of novel heterocyclic structures that can address these constraints and provide alternative therapeutic solutions [3].

Heterocyclic compounds are fundamental to contemporary drug discovery due to their structural variety and extensive range of biological activity [4]. Pyrimidine-based heterocycles and their fused counterparts have garnered considerable interest owing to their incorporation in various

clinically effective pharmaceuticals that have antibacterial, anticancer, antiviral, anti-inflammatory, and enzyme-inhibitory activities [5]. The pyrimidine nucleus, a crucial structural element of nucleic acids, exhibits remarkable compatibility with biological systems, rendering it a favored scaffold in medicinal research [6].

In this class, [1,2,4]triazolo[1,5-a]pyrimidines constitute a significant category of fused heterocycles recognized for their notable biological potential [7]. The amalgamation of triazole and pyrimidine rings results in stiff, planar structures that can form robust hydrogen bonds and π–π interactions with biological targets [8]. Numerous triazolo-pyrimidine derivatives have demonstrated significant antibacterial, antifungal, antitubercular, and kinase-inhibitory properties, underscoring their importance as foundational structures for therapeutic development.

The integration of supplementary pharmacophoric elements into this fused architecture is a recognized method to improve biological efficacy [9]. Pyridine moieties are well-known for enhancing binding affinity, balancing lipophilicity, and increasing membrane permeability of therapeutic candidates [10]. Pyridyl substitution frequently promotes coordination with active-site residues of microbial enzymes via nitrogen-based interactions, thus enhancing antimicrobial effectiveness [11]. The carboxamide functional group is a vital structural component in numerous bioactive compounds, offering hydrogen-bond donor and acceptor properties essential for stabilizing ligand–protein interactions [12].

This study aims to rationally create pyridyl-linked triazolo[1,5-a]pyrimidine-6-carboxamide derivatives by including three biologically relevant motifs: the triazolo-pyrimidine core, a pyridyl substituent, and a carboxamide connection [13]. This molecular hybridization method aims to produce drugs with improved antibacterial efficacy by synergistic interactions of the integrated pharmacophores [14].

This study presents the design, synthesis, structural characterisation, and in vitro antimicrobial assessment of a novel series of pyridyl-linked triazolo[1,5-a]pyrimidine-6-carboxamide derivatives [15-16]. The produced compounds were evaluated against specific Gram-positive and Gram-negative bacterial strains, together with fungal pathogens, to determine their antibacterial effectiveness [17]. The results of this study seek to offer significant insights for the creation of new heterocyclic antimicrobial drugs and establish a basis for more structural optimization and mechanistic research [18].

Experimental Work:

All reported melting points were determined using the open capillary tube method and are uncorrected [19]. The synthesis and analytical examination of the compounds were conducted with laboratory-grade and analytical-grade reagents, adhering to established procedures or previously reported methods, with modifications applied as necessary. Elemental analysis (C, H, and N) was conducted using a Perkin-Elmer model 240C analyzer, and all results aligned with theoretical values (within 0.4%) unless otherwise specified. 1H NMR spectra were acquired using the Bruker DPX-400 instrument operating at 400 MHz. The 1H chemical shifts are expressed in parts per million (ppm) relative to TMS (Me4Si). The LC mass spectra of the compounds were obtained using a Shimadzu 8201PC spectrometer [20]. The uniformity of the substances was assessed using ascending thin-layer chromatography (TLC) on silica gel G (Merck)-coated aluminum plates, observed with iodine vapor [21].

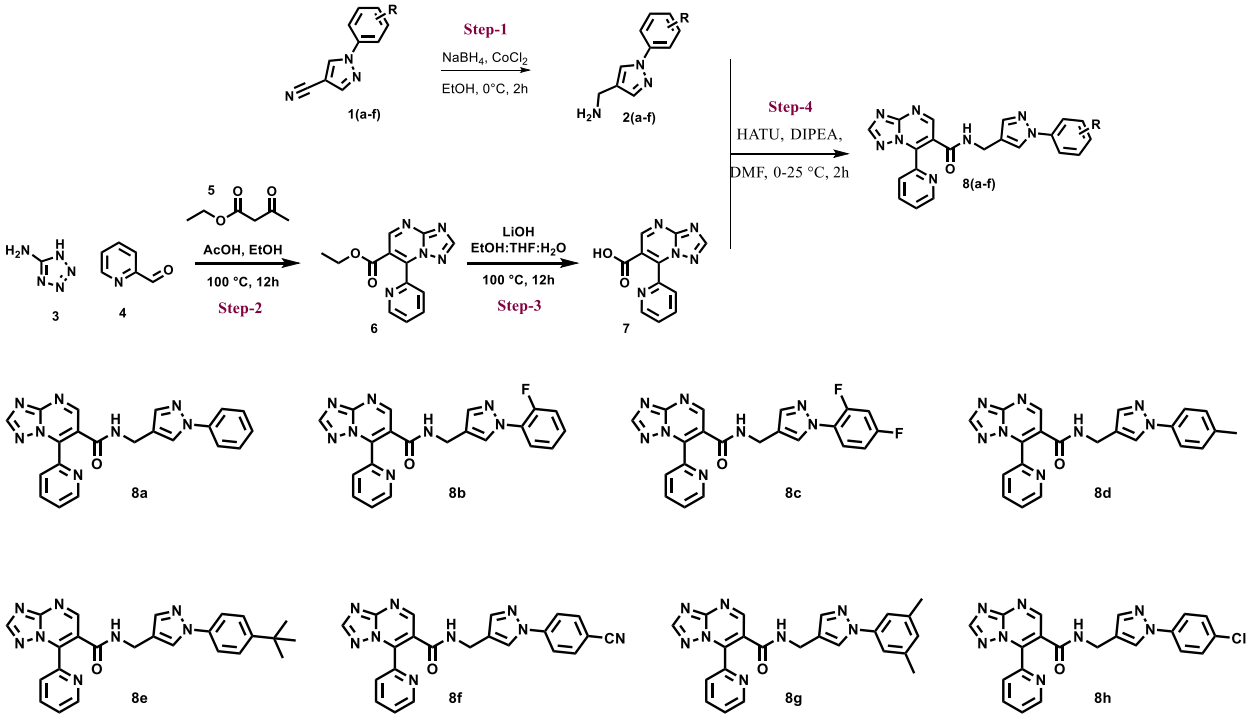

Scheme 1:

General procedure of synthesis of compounds 2a-2f:

The synthesis of compounds 2(a–f) was accomplished via the selective reduction of the nitrile group in the corresponding pyrazole-4-carbonitrile derivatives 1(a–f). The suitable starting

material 1(a–f) was dissolved in absolute ethanol, and cobalt (II) chloride (0.25 equivalents) was introduced to the solution. The reaction mixture was subsequently cooled to 0 °C with an ice bath to regulate the exothermic nature of the following phase [22]. Sodium borohydride was incrementally introduced to the agitated mixture over the course of 1 hour. Following the reaction's conclusion, as assessed by TLC, the reaction mixture was meticulously quenched with water and filtered through a Celite pad utilizing ethanol. The filtrate was concentrated at low pressure to eliminate ethanol, and the resultant aqueous layer was extracted with ethyl acetate. The amalgamated organic extracts were desiccated using anhydrous sodium sulfate and subsequently condensed under decreased pressure to yield the crude amine products 2(a–f). The crude products underwent additional purification via flash column chromatography to yield the required chemicals as pale yellow gums [23]. (2)

Synthesis of Compound 6:

The synthesis of chemical 6 was accomplished by a multi-component cyclocondensation reaction. A stirred solution of 5-amino-1H-tetrazole (3) (1.0 equivalent) in ethanol (EtOH), followed by the successive addition of picolinaldehyde (4) (1.0 equivalent) and ethyl acetoacetate (5) (1.5 equivalents), was prepared. A catalytic quantity of acetic acid (AcOH) was introduced to the mixture to promote the condensation [24]. The reaction mixture was heated to 100°C and held at this temperature for 12 hours. After the reaction was completed, as observed by TLC, the mixture was permitted to cool to ambient temperature. The solvent was removed under reduced pressure, and the resultant residue was purified to yield the triazolo pyrimidine derivative 6. The final product was obtained as a solid following suitable work-up and purification via flash column chromatography [25]. (2)

Synthesis of Compound 7:

A stirred solution of compound 6 (1.0 equivalent) in a mixture of ethanol, tetrahydrofuran, and water was treated with lithium hydroxide (LiOH, 3 equivalents). The reaction mixture was agitated at 25°C and sustained at this temperature for 6 hours. The reaction's progress was assessed via Thin-Layer Chromatography (TLC) until the total depletion of the starting material was noted [26]. The organic solvent was evaporated under reduced pressure. The residual aqueous solution was diluted with water and meticulously acidified (to pH 3 - 4) with the gradual addition of diluted

hydrochloric acid (HCl) at 0°C. The precipitate of carboxylic acid 7 was obtained using filtration, subsequently washed with water, and dried under vacuum conditions [27]. (2)

General procedure of synthesis of compounds 8a-8f:

A stirred solution of carboxylic acid derivative 7 (1.0 equiv.) in dimethylformamide (DMF) was treated with HATU (1.2 equiv.) and DIPEA (3.0 equiv.) at 0°C. The mixture was agitated for roughly 15 to 30 minutes at a constant temperature to promote acid activation [28]. Subsequently, the suitable amine derivative 2a-2f (1.0 equiv.) was included into the reaction mixture. The temperature incrementally increased to 25°C, and the agitation persisted for an additional 2 hours. The reaction's progress was assessed using thin-layer chromatography (TLC). Following completion, the reaction mixture was cooled with ice-cold water and subsequently extracted using ethyl acetate. The amalgamated organic layers were rinsed with brine, desiccated using anhydrous sodium sulfate, then concentrated under diminished pressure. The crude substance was purified via flash column chromatography to get the desired amide derivatives 8a-8f [29]. (2)

N-((1-phenyl-1H-pyrazol-4-yl)methyl)-7-(pyridin-2-yl)-[1,2,4]triazolo[1,5-a]pyrimidine-6-carboxamide (8a)

Melting Point: 208-210 ºC; Yield: 84 %; R_f value: 0.76; Solvent system: Benzene: Methanol (9:1); LCMS: m/z [M]+ 396.24; ^{1}H NMR ($CDCl_3$) δ ppm: 9.17 (s, 1H, Ar-H), 8.78-8.87 (d, 1H, Ar-H), 8.27 (s, 1H, Ar-H), 7.87-8.04 (m, 2H, Ar-H), 7.84 (s, 1H, NH), 7.32-7.82 (m, 8H, Ar-H), 4.24-4.30 (d, 2H, CH_2); Anal. Calcd. for $C_{21}H_{16}N_8O$ (396.41): C, 63.62%; H, 4.07%; N, 28.27%; Found: C, 63.63%; H, 3.95%; N, 28.00%

N-((1-(2-fluorophenyl)-1H-pyrazol-4-yl)methyl)-7-(pyridin-2-yl)-[1,2,4]triazolo[1,5-a]pyrimidine-6-carboxamide (8b)

Melting Point: 192-194 ºC; Yield: 84 %; R_f value: 0.73; Solvent system: Benzene: Methanol (9:1); LCMS: m/z [M]+ 414.21; ^{1}H NMR ($CDCl_3$) δ ppm: 9.49 (s, 1H, Ar-H), 8.78-8.86 (d, 1H, Ar-H), 8.27 (s, 1H, Ar-H), 7.53-8.01 (m, 6H, Ar-H), 7.50 (s, 1H, NH), 7.33-7.46 (m, 3H, Ar-H), 4.25(s, 2H, CH_2); Anal. Calcd. for $C_{21}H_{15}FN_8O$ (414.4): C, 60.86%; H, 3.65%; N, 27.05%; Found: C, 60.73%; H, 3.74%; N, 27.09%

N-((1-(2,4-difluorophenyl)-1H-pyrazol-4-yl)methyl)-7-(pyridin-2-yl)-[1,2,4]triazolo[1,5-a]pyrimidine-6-carboxamide (8c)

Melting Point: 202-204 ºC; Yield: 66 %; R_f value: 0.57; Solvent system: Benzene: Methanol (9:1); LCMS: m/z [M]+ 433.22; ^{1}H NMR ($CDCl_3$) δ ppm: 9.41 (s, 1H, Ar-H), 8.77-8.86 (d, 1H, Ar-H), 8.27 (s, 1H, Ar-H), 8.07 (s, 1H, NH), 6.96-7.97 (m, 9H, Ar-H), 4.22-4.30(d, 2H, CH_2); Anal. Calcd. for $C_{21}H_{14}F_2N_8O$ (432.39): C, 58.33%; H, 3.26%; N, 25.92%; Found: C, 58.28%; H, 3.26%; N, 25.93%.

7-(pyridin-2-yl)-N-((1-(p-tolyl)-1H-pyrazol-4-yl)methyl)-[1,2,4]triazolo[1,5-a]pyrimidine-6-carboxamide (8d)

Melting Point: 148-150 ºC; Yield: 85 %; R_f value: 0.67; Solvent system: Benzene: Methanol (9:1); LCMS: m/z [M]+ 410.09; ^{1}H NMR ($CDCl_3$) δ ppm: 9.39 (s, 1H, Ar-H), 8.69-8.78 (d, 1H, Ar-H), 8.27 (s, 1H, Ar-H), 7.07 (s, 1H, NH), 7.40-8.03 (m, 9H, Ar-H), 4.21-4.28(d, 2H, CH_2), 2.31 (s, 3H, CH_3); Anal. Calcd. for $C_{22}H_{18}N_8O$ (410.44): C, 64.37%; H, 4.42%; N, 27.31%; Found: C, 64.49%; H, 4.54%; N, 27.32%

N-((1-(4-(tert-butyl)phenyl)-1H-pyrazol-4-yl)methyl)-7-(pyridin-2-yl)-[1,2,4]triazolo[1,5-a]pyrimidine-6-carboxamide (8e)

Melting Point: 196-198 ºC; Yield: 80 %; R_f value: 0.62; Solvent system: Benzene: Methanol (9:1); LCMS: m/z [M]+ 452.28; ^{1}H NMR ($CDCl_3$) δ ppm: 9.70 (s, 1H, Ar-H), 8.84-8.93 (d, 1H, Ar-H), 8.27 (s, 1H, Ar-H), 7.40-8.03 (m, 9H, Ar-H), 6.66 (s, 1H, NH), 4.08-4.18(d, 2H, CH_2), 1.42 (s, 9H, CH_3); Anal. Calcd. for $C_{25}H_{24}N_8O$ (452.52): C, 66.35%; H, 5.35%; N, 24.77%; Found: C, 66.27%; H, 5.41%; N, 24.68%.

N-((1-(4-cyanophenyl)-1H-pyrazol-4-yl)methyl)-7-(pyridin-2-yl)-[1,2,4]triazolo[1,5-a]pyrimidine-6-carboxamide (8f)

Melting Point: 176-178 ºC; Yield: 67 %; R_f value: 0.76; Solvent system: Benzene: Methanol (9:1); LCMS: m/z [M]+ 421.27; ^{1}H NMR ($CDCl_3$) δ ppm: 9.37 (s, 1H, Ar-H), 8.71-8.80 (d, 1H, Ar-H), 8.21 (s, 1H, Ar-H), 8.03 (s, 1H, NH), 7.36-7.97 (m, 9H, Ar-H), 4.08-4.18(d, 2H, CH_2); Anal. Calcd. for $C_{22}H_{15}N_9O$ (421.42): C, 62.70%; H, 3.59%; N, 29.92%; Found: C, 63.07%; H, 3.75%; N, 29.97%.

N-((1-(3,5-dimethylphenyl)-1H-pyrazol-4-yl)methyl)-7-(pyridin-2-yl)-[1,2,4]triazolo[1,5-a]pyrimidine-6-carboxamide (8g)

Melting Point: 222-224 ºC; Yield: 82 %; R_f value: 0.68; Solvent system: Benzene: Methanol (9:1); LCMS: m/z [M]+ 425.32; ^{1}H NMR ($CDCl_3$) δ ppm: 9.26 (s, 1H, Ar-H), 8.81-8.88 (d, 1H, Ar-H), 8.27 (s, 1H, Ar-H), 7.82-8.05 (m, 3H, Ar-H), 7.79 (s, 1H, NH), 7.28-7.69 (m, 5H, Ar-H), 4.20-4.29 (d, 2H, CH_2), 2.33 (s, 6H, CH_3); Anal. Calcd. for $C_{23}H_{20}N_8O$ (424.47): C, 65.08%; H, 4.75%; N, 26.40%; Found: C, 65.24%; H, 5.06%; N, 26.57%.

N-((1-(4-chlorophenyl)-1H-pyrazol-4-yl)methyl)-7-(pyridin-2-yl)-[1,2,4]triazolo[1,5-a]pyrimidine-6-carboxamide (8h)

Melting Point: 254-256 ºC; Yield: 81 %; R_f value: 0.82; Solvent system: Benzene: Methanol (9:1); LCMS: m/z [M]+ 430.08; ^{1}H NMR ($CDCl_3$) δ ppm: 9.38 (s, 1H, Ar-H), 8.60-8.77 (d, 1H, Ar-H), 8.27 (s, 1H, Ar-H), 7.42-8.03 (m, 7H, Ar-H), 7.38 (s, 1H, NH), 7.29-7.36 (m, 2H, Ar-H), 4.24-4.35 (d, 2H, CH_2); Anal. Calcd. for $C_{21}H_{15}ClN_8O$ (430.86): C, 58.54%; H, 3.51%; N, 26.01%; Found: C, 58.37%; H, 3.75%; N, 25.99%.

.2 *In vitro* Antimicrobial Activity

The synthesized compounds (8a-8h) were evaluated for antibacterial activity using the cup plate method to ascertain the zone of inhibition.

Materials:

Two gram-positive bacterial strains, Staphylococcus aureus and Bacillus anthracis, together with two gram-negative bacterial strains, Pseudomonas aeruginosa and Escherichia coli, were utilized to assess antibacterial activity. Two fungal strains, C. albicans and A. niger, were utilized to assess antifungal activity [30]. Ciprofloxacin and Fluconazole served as the standards for antibacterial and antifungal activity, respectively. DMSO served as the solvent control. Nutrient broth served as the culture medium for bacteria, whereas Sabouraud dextrose broth was utilized for fungi [31].

Method:

Sterile nutrition broth and Sabouraud dextrose broth plates were made by putting sterile agar into Petri dishes under aseptic circumstances. 0.1 ml of each standardized test organism was put onto agar plates. Holes were created utilizing a sterile borer with a diameter of 6 mm. The test drug, the reference drug, and the solvent control were individually inserted in each well [32]. The plates

were subsequently kept at 4 °C for 1 hour to facilitate the diffusion of the solution into the medium. All bacterial plates were incubated at 37 °C for 24 hours, whereas fungal plates were incubated at 25 °C for 48 hours. The inhibitory zone was quantified in millimeters [33]. (4)

***In silico* ADME study**

The ADME characteristics of the synthesized compounds (8a-8h) were assessed using the publicly accessible SwissADME web server (http://www.swissadme.ch). SMILES strings for each molecule were initially produced from the finalized, curated 2D structures (created in ChemDraw) and subsequently validated through back-rendering to confirm accurate connectivity and protonation state (neutral at pH 7.4 unless a different predominant state was indicated by pKa). Each molecule's SMILES notation was entered into the SwissADME input field (one entry per line, with molecule names prefixed for identification, e.g., “2a <space> SMILES”), and the job was submitted using default parameters. SwissADME autonomously calculates various lipophilicity estimators; for the purpose of reporting a singular value, the iLOGP (consensus fragmental/logS-based lipophilicity model) was chosen, and the "consensus LogP" was qualitatively examined to confirm the absence of significant discrepancies across models. Upon completion of the calculations, the results page was preserved as a PDF, and a CSV export was downloaded for archival purposes [34].

The SwissADME output yielded the following descriptors, which were documented in the study datasheet: molecular weight (MW), number of rotatable bonds, hydrogen-bond acceptors (HBA) and donors (HBD), topological polar surface area (TPSA), iLOGP, gastrointestinal (GI) absorption category (“High” or “Low” as determined by the BOILED-Egg model), and the count of violations of Lipinski’s rule-of-five (Ro5). The interactive "BOILED-Egg" image was utilized to verify the positioning of the white zone (indicating high intestine absorption) vs the yellow zone (indicating blood-brain barrier permeability); only the categorization pertaining to intestinal absorption is provided here. The "bioavailability radar" was examined as necessary to contextualize the overall drug-likeness, including polarity, size, lipophilicity, solubility, flexibility, and saturation; however, the numerical reporting prioritized the aforementioned descriptors to maintain consistency with our dataset [35].

The evaluation of Lipinski compliance was conducted as outlined below: MW ≤ 500, iLOGP (or consensus LogP) ≤ 5, HBA ≤ 10, HBD ≤ 5; substances satisfying a minimum of four criteria were

classified as Ro5-compliant (0 violations recorded by SwissADME). The Topological Polar Surface Area (TPSA) was employed to elucidate passive permeability: TPSA values < 90 Å² typically promote favorable intestinal absorption, whereas values ≥ 120 Å² frequently suggest diminished passive diffusion. The quantity of rotatable bonds (≤10) was monitored to assess molecular flexibility pertinent to oral bioavailability. All values were simply translated from SwissADME without manual recalibration [36]. Discrepancies between internal calculators and SwissADME were handled in favor of SwissADME to ensure methodological consistency.

Molecular Docking Study

Hardware and Software:

The docking process was executed on a Windows 10 (64-bit) operating system equipped with 4 GB of RAM and a 2.50 GHz Intel(R) Core(TM) i5-7200U CPU. PyRx version 0.8, accessible at https://pyrx.sourceforge.io/, was utilized to do the docking in AutoDock Vina Wizard. Autodock Tools 4.2.6, provided by the Scripps Research Institute at https://autodock.scripps.edu/, was utilized for protein preparation and grid generation. Ligands were processed with Open Babel and PyRx 0.8, while interaction poses of ligands were visualized and analyzed using Discovery Studio Visualizer.

Selection of Target Proteins: Molecular docking experiments of compounds 8a-8h and 11a-11h were conducted on two microbial proteins to evaluate their antibacterial properties [37]. PDB ID: 1KZN - The crystal structure of the 24 kDa domain of E. coli in combination with clorobiocin was selected.

Protein and ligand processing for docking

Protein Preparation

The crystal structures of target proteins (PDB ID: 1KZN - Crystal Structure of E. coli 24kDa Domain in Complex with Clorobiocin) were obtained from the RCSB Protein Data Bank, and the proteins were produced utilizing Autodock Tools 4.2.6. In this phase, associated water molecules and bonded heteroatoms/ligands were eliminated, polar hydrogens and Kollman charges were included, the charge was uniformly distributed across all atoms, and residues were examined for any missing atoms. The produced PDB files were subsequently translated to the PDBQT format for the following phase of execution [38].

Ligand Processing

Ligands in SMILES format were transformed into SDF files, and three-dimensional coordinates for all ligands were created with Open Babel via the command line [39]. The 3D structural data files were processed in PyRx with UFF energy minimization and subsequently translated to PDBQT format (a format recognizable by Autodock).

Grid Generation

The grid box was initially positioned over the linked ligands via AutoDock Tools and subsequently refined to the required dimensions in PyRx [40]. The grid dimensions were established at 19.150 x 30.393 x 34.745 $Å^3$, with 25 points allocated in the X, Y, and Z directions for PDB ID: 1KZN.

Docking and visualization of results:

The docking was executed in the Vina Wizard of the PyRx Tool, employing an exhaustiveness setting of 8, and the resulting output files were divided into separate pose files. The data and protein structure were subsequently utilized for interaction visualization via Discovery Studio Visualizer [41].

Results and Discussion

Chemistry

The synthetic strategy employed in this study successfully enabled the construction of a novel series of pyridyl-linked triazolo[1,5-a]pyrimidine-6-carboxamide derivatives (8a–8h) through a rational, stepwise approach. The overall chemistry was designed to ensure structural diversity at the amide side chain while preserving the biologically significant triazolo-pyrimidine core. The synthesis proceeded smoothly through the key intermediates, culminating in the formation of the target compounds in moderate to excellent yields (66–85%), indicating the robustness and reproducibility of the adopted methodology. The multicomponent cyclocondensation used for constructing the triazolo[1,5-a]pyrimidine nucleus proved efficient, affording the core scaffold without requiring harsh conditions or prolonged reaction times. Subsequent hydrolysis and amide coupling reactions using HATU/DIPEA conditions facilitated clean conversion to the final carboxamide derivatives, highlighting the suitability of this coupling protocol for structurally complex heterocycles. The reaction conditions were found to be tolerant of a variety of substituents on the pyrazolyl phenyl ring, including electron-donating (methyl, tert-butyl) and electron-withdrawing (fluoro, chloro, cyano) groups. This functional group tolerance underscores the

synthetic flexibility of the route and allows systematic structure–activity investigations. All synthesized compounds were thoroughly characterized using melting point determination, TLC analysis, ^{1}H NMR spectroscopy, LC-MS, and elemental analysis. The sharp melting points and single TLC spots for each compound confirmed their purity and homogeneity. Elemental analysis data (C, H, N) were in close agreement with the calculated values (±0.4%), providing strong confirmation of the proposed molecular formulas. The ^{1}H NMR spectra of compounds 8a–8h consistently displayed characteristic signals corresponding to the triazolo-pyrimidine framework. The downfield singlets observed around δ 9.1–9.7 ppm were attributed to aromatic protons of the fused heterocyclic system, while the amide NH proton resonated as a singlet in the range of δ 6.6–8.1 ppm, confirming successful amide bond formation. The methylene protons (–CH_2–) linking the pyrazole ring to the amide nitrogen appeared as distinct doublets or singlets around δ 4.0–4.3 ppm, further validating the connectivity. Aromatic protons from phenyl and pyridyl moieties appeared as multiplets within the expected δ 7.0–8.0 ppm region, with substitution patterns clearly reflected in signal multiplicity and integration.

***In vitro* antimicrobial activity**

The *in vitro* antimicrobial activity of the synthesized pyridyl-linked triazolo[1,5-a]pyrimidine-6-carboxamide derivatives (8a–8h) was evaluated against selected Gram-positive bacteria (*Staphylococcus aureus*, *Bacillus anthracis*), Gram-negative bacteria (*Pseudomonas aeruginosa*, *Escherichia coli*), and fungal strains (*Candida albicans*, *Aspergillus niger*) using the cup plate diffusion method at a concentration of 1000 µg/ml. The results, expressed as zones of inhibition (mm), are summarized in Table 1 and compared with standard drugs ciprofloxacin (antibacterial) and fluconazole (antifungal).

Overall, the synthesized compounds exhibited moderate to good antimicrobial activity, indicating that the triazolo[1,5-a]pyrimidine framework, when substituted with appropriate aryl/heteroaryl moieties, contributes positively to microbial growth inhibition. Among the tested series, compounds 8d and 8g emerged as the most potent derivatives across both bacterial and fungal strains. Compound 8d displayed zones of inhibition ranging from 23–25 mm against bacterial strains and 21–22 mm against fungal strains, approaching the activity of ciprofloxacin and fluconazole. Similarly, compound 8g showed consistently high inhibition (21–23 mm for bacteria and 19–20 mm for fungi), highlighting its broad-spectrum antimicrobial potential.

Compounds 8b, 8c, and 8h demonstrated good antibacterial activity, particularly against *S. aureus* and *E. coli*, with inhibition zones in the range of 19–22 mm. Their antifungal activity was moderate but significant, suggesting that halogen substitution (fluoro or chloro groups) on the phenyl ring enhances lipophilicity and facilitates better interaction with microbial targets. In contrast, compounds 8a, 8e, and 8f exhibited comparatively lower activity, with inhibition zones mostly between 14–18 mm. The reduced potency of these derivatives may be attributed to less favorable electronic effects or steric hindrance arising from their respective substituents, which could limit optimal binding to microbial enzymes.

A structure–activity relationship (SAR) analysis indicates that electron-donating groups such as methyl substituents (as in 8d and 8g) significantly improve antimicrobial efficacy, possibly by enhancing membrane permeability and stabilizing ligand–target interactions. Conversely, bulky substituents like tert-butyl (8e) or strongly electron-withdrawing groups such as cyano (8f) appear to diminish activity, likely due to steric constraints or altered electronic distribution affecting binding affinity. In comparison with the standard drugs, none of the synthesized compounds surpassed ciprofloxacin or fluconazole; however, several derivatives—particularly 8d and 8g—exhibited inhibition zones close to those of the reference compounds. This observation underscores the promise of the triazolo[1,5-a]pyrimidine scaffold as a viable lead structure for further optimization.

Table 1: *In vitro* antimicrobial activity of compounds 8a-8h

Compound (1000 µg/ml)	**Zone of Inhibition (mm)**					
	S. aureus	***B. anthracis***	***P. aeruginosa***	***E. coli***	***C. albicans***	***A. niger***
Ciprofloxacin	**30**	**29**	**28**	**30**	–	–
Fluconazole	–	–	–	–	**28**	**27**
8a	16	15	14	15	14	13
8b	22	21	20	21	19	18
8c	21	20	19	20	18	17
8d	25	24	23	24	22	21
8e	17	16	15	16	15	14

8f	18	17	16	17	15	15
8g	23	22	21	22	20	19
8h	21	20	19	20	18	17

***In silico* ADME**

All compounds in the series exhibited molecular weights in the range of 396.41–452.52 g/mol, remaining within the acceptable limit (<500 g/mol) prescribed by Lipinski's rule. This suggests favorable prospects for oral drug development. The number of hydrogen-bond acceptors (8–9) and hydrogen-bond donors (1) for all derivatives also satisfied the Ro5 criteria, indicating an appropriate balance between polarity and permeability. The rotatable bond count (5–7) for the synthesized molecules falls well below the recommended threshold (≤10), reflecting moderate molecular flexibility, which is advantageous for conformational adaptation within biological targets without excessive entropic penalties.

The topological polar surface area (TPSA) values for most compounds were approximately 102.89 Å², while compound 8f showed a slightly higher TPSA of 126.68 Å². TPSA values below ~120 Å² are generally associated with good intestinal absorption, and accordingly, SwissADME predicted high GI absorption for all compounds, including 8f. This indicates that despite its higher polarity, compound 8f may still retain acceptable oral absorption characteristics.

Lipophilicity, expressed as iLOGP, ranged from 2.17 to 3.60 across the series. These moderate lipophilicity values are considered optimal for oral drugs, as excessively lipophilic compounds may suffer from poor solubility and rapid metabolic clearance, whereas overly hydrophilic molecules often show limited membrane permeability. The slightly higher iLOGP value observed for compound 8e (3.6) can be attributed to the presence of a tert-butyl substituent, which increases hydrophobic character; however, it still remains within the acceptable Ro5 range.

Importantly, none of the compounds exhibited any Lipinski violations, underscoring their overall drug-likeness and suitability for further development as orally active antimicrobial agents. The collective ADME profile indicates that the incorporation of the triazolo[1,5-a]pyrimidine core, pyridyl moiety, and carboxamide linkage results in molecules with balanced physicochemical properties, combining adequate polarity with sufficient lipophilicity.

Table 2: *In silico* ADME of compounds 8a-8h

Comp	Molecular Weight	Rotatable bonds	H-bond acceptors	H-bond donors	TPSA	iLOGP	GI absorption	Lipinski violations
8a	396.41	5	8	1	102.89	2.3	High	0
8b	414.4	5	8	1	102.89	2.44	High	0
8c	432.39	5	8	1	102.89	2.58	High	0
8d	410.44	6	8	1	102.89	2.61	High	0
8e	452.52	5	8	1	102.89	3.6	High	0
8f	421.42	5	9	1	126.68	2.17	High	0
8g	424.47	7	8	1	102.89	2.92	High	0
8h	430.86	5	8	1	102.89	2.96	High	0

Molecular Docking Study:

To rationalize the observed *in vitro* antimicrobial activity and to gain insight into the possible binding mode of the synthesized compounds, a molecular docking study was performed for compounds 8a–8h against the bacterial target protein E. coli 24 kDa domain (PDB ID: 1KZN) using AutoDock Vina via the PyRx platform. Ciprofloxacin was used as the reference ligand for comparative interaction analysis. The docking results, including binding affinity, ligand efficiency, predicted inhibition constant (Ki), and key amino acid interactions, are summarized in Tables 3 and 4. All synthesized compounds exhibited favorable binding affinities toward the selected protein target, with docking scores ranging from –7.9 to –8.9 kcal/mol, indicating strong and energetically stable ligand–protein complexes. Among the tested series, compound 8d showed the highest binding affinity (–8.9 kcal/mol), followed closely by 8g (–8.7 kcal/mol) and 8b/8c (–8.5 kcal/mol). These results correlate well with the *in vitro* antimicrobial data, where compounds 8d and 8g also demonstrated superior biological activity. The ligand efficiency values (–0.23 to –0.29 kcal/mol/NHA) further support the efficient utilization of non-hydrogen atoms in stabilizing the ligand–protein complex. Compound 8d exhibited the highest ligand efficiency (–0.29), suggesting optimal interactions per atom and reinforcing its potential as a lead compound. The predicted inhibition constants (Ki) were in the nanomolar range (299–1619 nM), with compound 8d again

showing the lowest Ki value (299.4 nM), indicative of strong inhibitory potential. Detailed interaction analysis revealed that all compounds were well accommodated within the active site of the target protein, engaging in a combination of hydrogen bonding, hydrophobic interactions, and electrostatic contacts with key amino acid residues. Common interacting residues across the compound series included GLU 50, ASP 73, ASN 46, ALA 47, VAL 120, ILE 78, ARG 76, and GLY 77, many of which are also involved in the binding of the standard drug ciprofloxacin. This overlap suggests that the synthesized compounds may inhibit the protein through a mechanism similar to that of established antibacterial agents. Compound 8d, the most potent docked ligand, interacted with critical residues such as GLU 50, ASN 46, ASP 73, ARG 76, VAL 120, and ILE 78, forming a dense interaction network within the binding pocket. The presence of a *p*-tolyl substituent likely enhances hydrophobic contacts, thereby stabilizing the ligand within the active site. Similarly, compound 8g, bearing dimethyl substitutions, formed strong interactions with ARG 76, GLU 50, ASP 49, ASN 46, and VAL 120, supporting its high docking score and biological efficacy. Halogenated derivatives such as 8b, 8c, and 8h also demonstrated stable binding, where fluorine and chlorine substitutions contributed to favorable hydrophobic and van der Waals interactions without disrupting hydrogen-bond networks. In contrast, compound 8e, despite having a bulky tert-butyl group, showed slightly reduced binding affinity (–7.9 kcal/mol), possibly due to steric hindrance within the binding pocket, which may limit optimal orientation.

A good correlation was observed between docking scores and experimental antimicrobial activity. Compounds with higher binding affinities and lower Ki values (8d, 8g, 8b) generally exhibited stronger *in vitro* antimicrobial effects, whereas compounds with comparatively weaker docking scores showed moderate biological activity. This consistency validates the docking protocol and supports the hypothesis that inhibition of the selected bacterial protein may contribute to the antimicrobial mechanism of action of these compounds. The molecular docking study confirms that the pyridyl-linked triazolo[1,5-a]pyrimidine-6-carboxamide scaffold is well-suited for interaction with bacterial protein targets. The combined presence of hydrogen-bond donors/acceptors, aromatic systems for π–π stacking, and appropriately tuned lipophilicity enables effective binding within the active site. Among the series, compound 8d emerges as the most promising lead, supported by superior docking parameters, extensive residue interactions, and strong agreement with *in vitro* antimicrobial results.

Table 3: Results of Molecular Docking of Compounds 8a-8h against PDB id: 1KZN

Ligand	Affinity (Kcal/mol)	Ligand Efficiency (kcal/mol/NHA)	Ki (nM)
8a	-8	-0.27	1367.6
8b	-8.5	-0.27	588.11
8c	-8.5	-0.27	588.11
8d	-8.9	-0.29	299.4
8e	-7.9	-0.23	1619.05
8f	-8.2	-0.26	975.79
8g	-8.7	-0.27	419.62
8h	-8.4	-0.27	696.24

Table 4: Binding Interactions of Compounds 8a-8h against PDB id: 1KZN

Ligand	Interactions	H-bond
8a	ALA 47, ASN 46, VAL 120, GLY 117, GLU 42, ASP 49, GLU 50, ILE 78, GLY 77, ARG 136, ARG 76, ASP 73.	
8b	ASP 73, THR 165, VAL 167, VAL 43, ASN 46, ALA 47, ILE 78, GLU 50, GLY 119, VAL 120, SER 121, HIS 95, ALA 96.	
8c	GLU 50, ASP 49, ALA 47, ASN 46, ASP 45, GLU 42, GLY 119, GLY 117, ILE 78, GLY 77, ARG 76, ARG 136, ASP 73.	
8d	GLU 50, ALA 47, ASN 46, VAL 120, VAL 43, VAL 71, ASP 73, VAL 167, ARG 76, GLY 77, ILE 78, PRO 79, ARG 136.	

8e	GLU 50, ASP 49, ALA 47, ASN 46, VAL 43, ASP 73, VAL 71, VAL 167, MET 166, THR 165, GLY 119, VAL 120, HIS 95, ALA 96, ILE 78.	
8f	PRO 79, ILE 78, GLY 77, ARG 76, THR 165, ASP 73, VAL 120, ASN 46, GLU 50.	
8g	ARG 76, GLY 77, ILE 78, PRO 79, GLU 50, ASP 49, ALA 47, ASN 46, VAL 120, VAL 167, THR 165, VAL 71, ASP 73.	
8h	VAL 120, GLY 117, ALA 96, ASP 49, ASN 46, VAL 43, GLU 42, ILE 78, THR 165, VAL 167, ASP 73, VAL 71.	
Ciprofloxacin	VAL 120, ASP 73, ARG 76, GLY 77, ILE 78, THR 165, GLU 50, ALA 47, ASN 46.	VAL 43

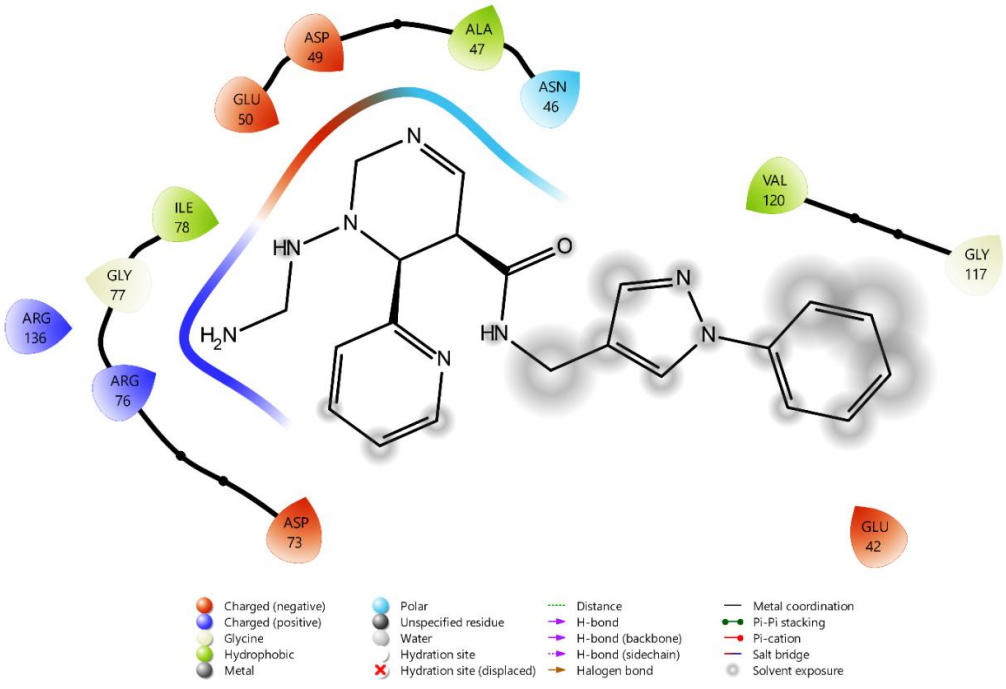

8a-1KZN

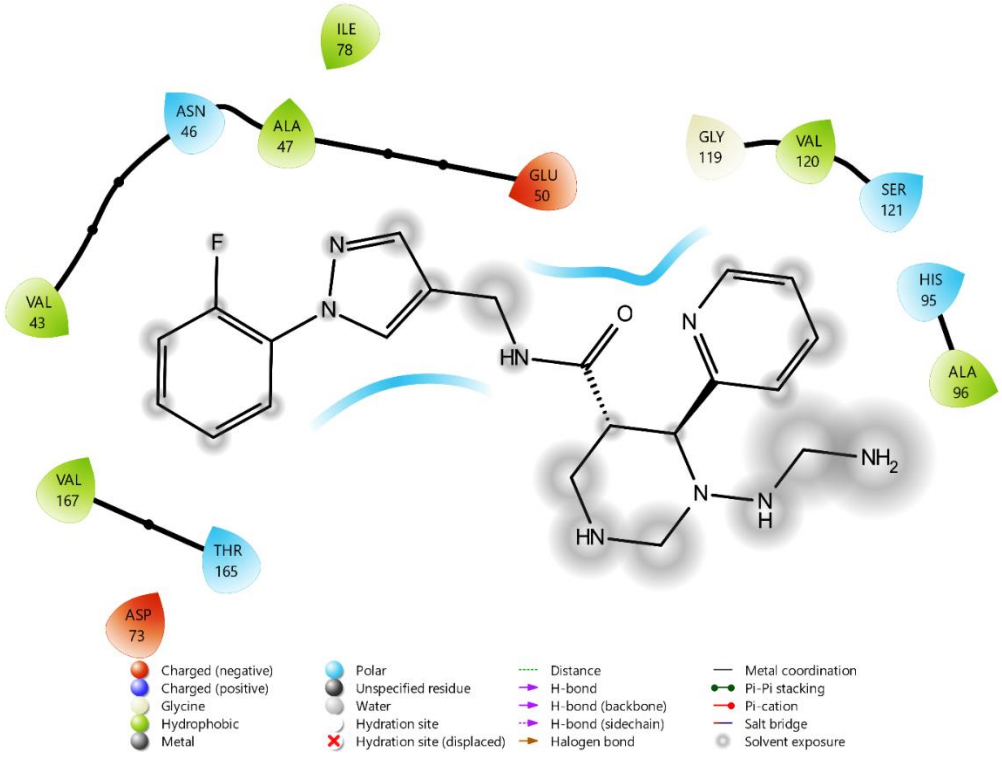

8b-1KZN

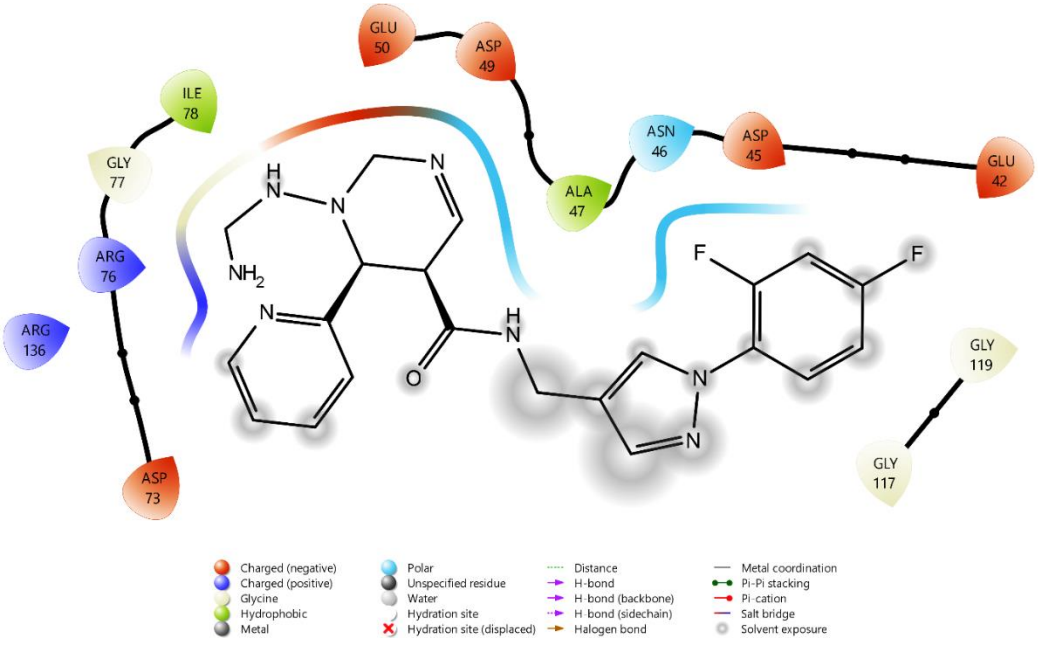

8c-1KZN

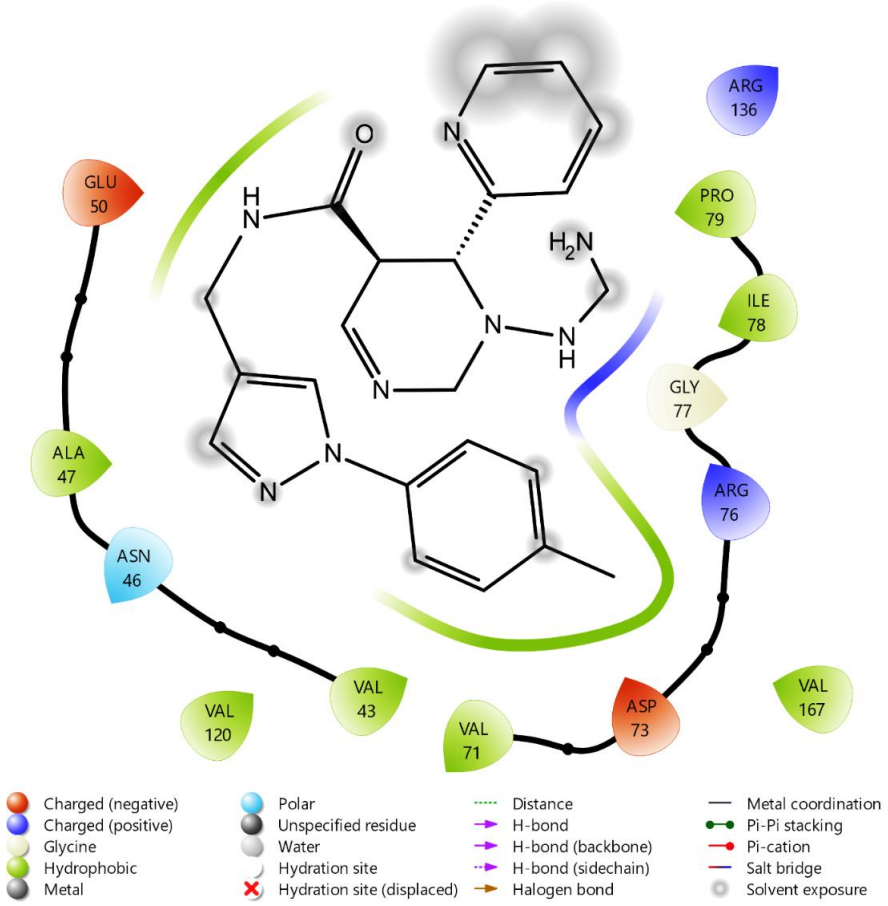

8d-1KZN

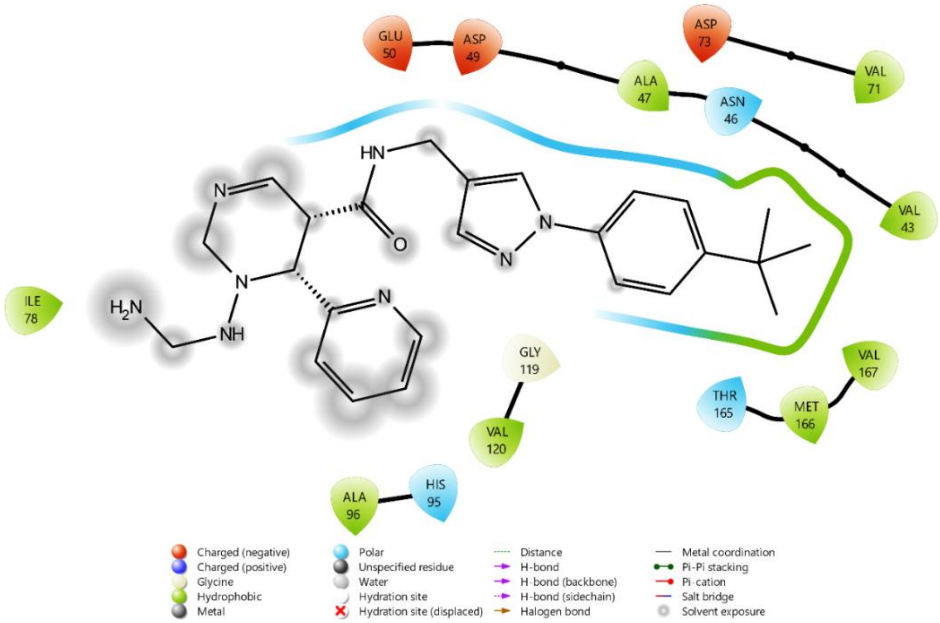

8e-1KZN

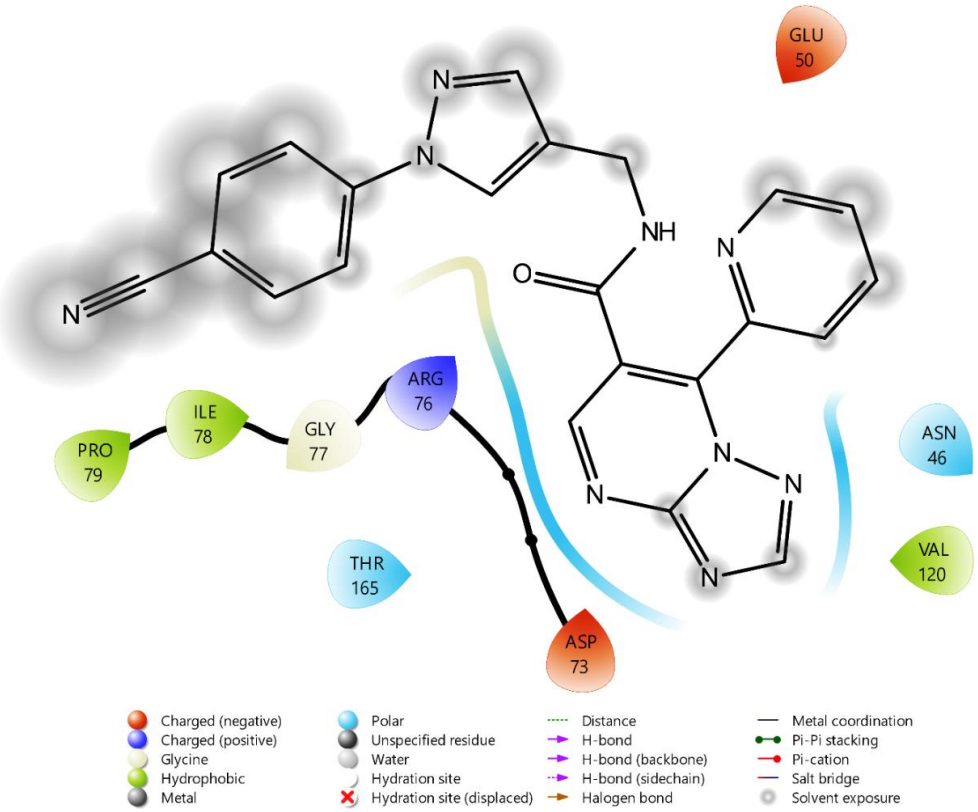
GLU 50
ARG 76
ILE 78
GLY 77
PRO 79
ASN 46
VAL 120
THR 165
ASP 73
Charged (negative)
Charged (positive)
Glycine
Hydrophobic
Metal
Polar
Unspecified residue
Water
Hydration site
Hydration site (displaced)
Distance
H-bond
H-bond (backbone)
H-bond (sidechain)
Halogen bond
Metal coordination
Pi-Pi stacking
Pi-cation
Salt bridge
Solvent exposure

8f-1KZN

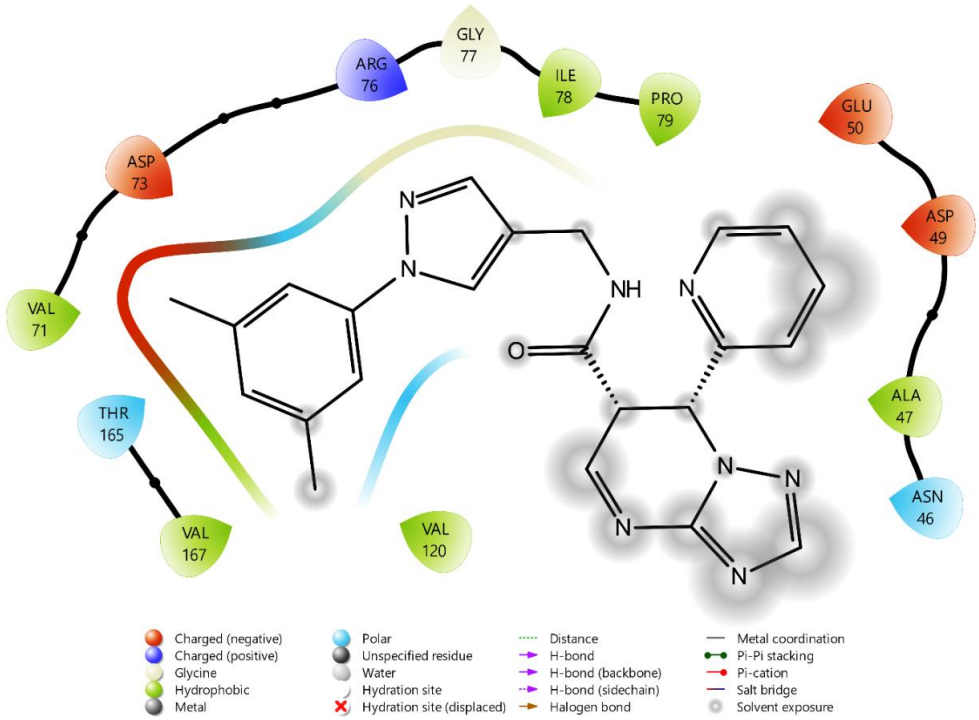
GLY 77
ARG 76
ILE 78
PRO 79
ASP 73
GLU 50
ASP 49
VAL 71
THR 165
ALA 47
ASN 46
VAL 167
VAL 120
Charged (negative)
Charged (positive)
Glycine
Hydrophobic
Metal
Polar
Unspecified residue
Water
Hydration site
Hydration site (displaced)
Distance
H-bond
H-bond (backbone)
H-bond (sidechain)
Halogen bond
Metal coordination
Pi-Pi stacking
Pi-cation
Salt bridge
Solvent exposure

8g-1KZN

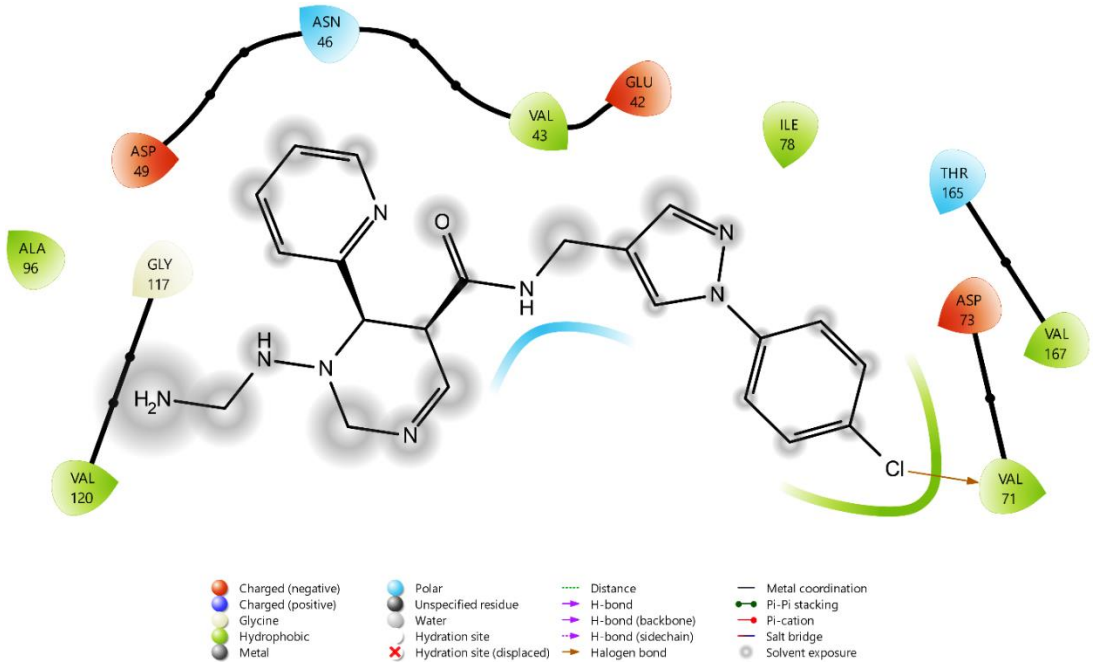

8h-1KZN

Conclusion

In the present study, a novel series of pyridyl-linked triazolo[1,5-a]pyrimidine-6-carboxamide derivatives (8a–8h) was successfully designed, synthesized, and characterized using standard analytical techniques. The synthesized compounds exhibited moderate to good *in vitro* antimicrobial activity, with compounds 8d and 8g emerging as the most promising candidates. *In silico* ADME analysis confirmed favorable drug-likeness and oral bioavailability profiles for all derivatives. Molecular docking studies revealed strong binding affinities with the selected bacterial target, supporting the experimental antimicrobial findings. Overall, the results highlight the triazolo[1,5-a]pyrimidine scaffold as a potential lead framework for the development of new antimicrobial agents.

References

1. Bassetti M, Poulakou G, Ruppe E, Bouza E, Van Hal SJ, Brink A. Antimicrobial resistance in the next 30 years, humankind, bugs and drugs: a visionary approach. Intensive care medicine. 2017 Oct;43(10):1464-75.

2. Wright GD. Bacterial resistance to antibiotics: enzymatic degradation and modification. Advanced drug delivery reviews. 2005 Jul 29;57(10):1451-70.

3. Taylor AP, Robinson RP, Fobian YM, Blakemore DC, Jones LH, Fadeyi O. Modern advances in heterocyclic chemistry in drug discovery. Organic & biomolecular chemistry. 2016;14(28):6611-37.

4. Taylor AP, Robinson RP, Fobian YM, Blakemore DC, Jones LH, Fadeyi O. Modern advances in heterocyclic chemistry in drug discovery. Organic & biomolecular chemistry. 2016;14(28):6611-37.

5. Vyas A, Sahu B, Pathania S, Nandi NK, Chauhan G, Asati V, Kumar B. An insight on medicinal attributes of pyrimidine scaffold: An updated review. Journal of Heterocyclic Chemistry. 2023 Jul;60(7):1081-121.

6. Vyas A, Sahu B, Pathania S, Nandi NK, Chauhan G, Asati V, Kumar B. An insight on medicinal attributes of pyrimidine scaffold: An updated review. Journal of Heterocyclic Chemistry. 2023 Jul;60(7):1081-121.

7. Pinheiro S, Pinheiro EM, Muri EM, Pessôa JC, Cadorini MA, Greco SJ. Biological activities of [1, 2, 4] triazolo [1, 5-a] pyrimidines and analogs. Medicinal Chemistry Research. 2020 Oct;29(10):1751-76.

8. Guan Q, Xing S, Wang L, Zhu J, Guo C, Xu C, Zhao Q, Wu Y, Chen Y, Sun H. Triazoles in medicinal chemistry: physicochemical properties, bioisosterism, and application. Journal of Medicinal Chemistry. 2024 May 3;67(10):7788-824.

9. Meanwell NA. Improving drug design: an update on recent applications of efficiency metrics, strategies for replacing problematic elements, and compounds in nontraditional drug space. Chemical Research in Toxicology. 2016 Apr 18;29(4):564-616.

10. Tyagi S, Mishra R, Mazumder R, Mazumder A. Current Market Potential and Prospects of Copper-based Pyridine Derivatives: A Review. Current Molecular Medicine. 2024 Sep 1;24(9):1111-23.

11. Claudel M, Schwarte JV, Fromm KM. New antimicrobial strategies based on metal complexes. Chemistry. 2020 Oct 16;2(4):849-99.

12. Kumari S, Carmona AV, Tiwari AK, Trippier PC. Amide bond bioisosteres: Strategies, synthesis, and successes. Journal of medicinal chemistry. 2020 Jul 20;63(21):12290-358.

13. Baraldi PG, Tabrizi MA, Romagnoli R, El-Kashef H, Preti D, Bovero A, Fruttarolo F, Gordaliza M, Borea PA. Pyrazolo [4, 3-e][1, 2, 4] triazolo [1, 5-c] pyrimidine template: organic and medicinal chemistry approach. Current Organic Chemistry. 2006 Feb 1;10(3):259-75.

14. de Sena Murteira Pinheiro P, Franco LS, Montagnoli TL, Fraga CA. Molecular hybridization: a powerful tool for multitarget drug discovery. Expert Opinion on Drug Discovery. 2024 Apr 2;19(4):451-70.

15. Chhabra S, Shah K. The novel scaffold 1, 2, 4-benzothiadiazine-1, 1-dioxide: a review. Medicinal Chemistry Research. 2021 Jan;30(1):15-30.

16. Patel G, Ghumara R, Patel S, Shah P, Patel N, Lunagariya N, Mali S, Patel M, Shah U. Molecular docking, dynamics, and cytotoxicity assessment of pyrazolo[1,5-a]pyrimidine derivatives against breast cancer. Chem Biodivers. 2025 Sep 17;e01510.

17. Shah P. Synthesis and molecular docking study of a series of novel pyridine derivatives and evaluation of their anticancer activity. J Pharm Res Int [Internet]. 2025 Sep 18 [cited 2025 Nov 21];37(9):97–107.

18. Taylor AP, Robinson RP, Fobian YM, Blakemore DC, Jones LH, Fadeyi O. Modern advances in heterocyclic chemistry in drug discovery. Organic & biomolecular chemistry. 2016;14(28):6611-37.

19. Deman JM, Deman L, Blackman B. Melting-point determination of fat products. Journal of the American Oil Chemists' Society. 1983 Jan;60(1):91-4.

20. Yener I, Ertaş A, Yilmaz MA, Tokul Ölmez Ö, Köseoğlu Yılmaz P, Yeşil Y, Kaplaner E, Öztürk M, Temel H, Kolak U, Topçu G. Characterization of the chemical profile of Euphorbia species from Turkey by gas chromatography–mass spectrometry (GC-MS), liquid chromatography–tandem mass spectrometry (LC-MS/MS), and liquid chromatography–ion trap–time-of-flight–mass spectrometry (LC-IT-TOF-MS) and chemometric analysis. Analytical Letters. 2019 May 3;52(7):1031-49.

21. Viradiya R, Patel M, Rohit S, Shah U, Patel G, Vashi A, et al. Unveiling the potential of morpholinium surface active ionic liquids for epidermal growth factor receptor inhibition: synthesis, integrating molecular docking, dynamics, and *in vitro* studies. ACS Omega. 2025;10(20):20562–20569.

22. Rahier H, Wastiels J, Biesemans M, Willlem R, Van Assche G, Van Mele B. Reaction mechanism, kinetics and high temperature transformations of geopolymers. Journal of materials science. 2007 May;42(9):2982-96.

23. Jahanbin K, Moini S, Gohari AR, Emam-Djomeh Z, Masi P. Isolation, purification and characterization of a new gum from Acanthophyllum bracteatum roots. Food hydrocolloids. 2012 May 1;27(1):14-21.

24. Panov AG, Fripiat JJ. Acetone condensation reaction on acid catalysts. Journal of Catalysis. 1998 Aug 15;178(1):188-97.

25. Tzschucke CC, Markert C, Bannwarth W, Roller S, Hebel A, Haag R. Modern separation techniques for the efficient workup in organic synthesis. Angewandte Chemie International Edition. 2002 Nov 4;41(21):3964-4000.

26. Hemmateenejad B, Akhond M, Mohammadpour Z, Mobaraki N. Quantitative monitoring of the progress of organic reactions using multivariate image analysis-thin layer chromatography (MIA-TLC) method. Analytical Methods. 2012;4(4):933-9.

27. Bai F, Yang X, Li R, Huang B, Huang W. Monodisperse hydrophilic polymer microspheres having carboxylic acid groups prepared by distillation precipitation polymerization. Polymer. 2006 Jul 26;47(16):5775-84.

28. Diao Y, Walawender WP, Fan LT. Activated carbons prepared from phosphoric acid activation of grain sorghum. Bioresource technology. 2002 Jan 1;81(1):45-52.

29. Tkachuk VA, Hordiyenko OV, Omelchenko IV, Medviediev VV, Arrault A. Methyl esters of 2-(N-hydroxycarbamimidoyl) benzoyl-substituted α-amino acids as promising building blocks in peptidomimetic synthesis: a comparative study. Monatshefte für Chemie-Chemical Monthly. 2018 Dec;149(12):2293-309.

30. Rahimifard N, Shoeibi S, Pakzad SR, HajimehdipoOr H, Sabzevari O, AjdarY S. Antifungal activity of the essential oil of Eugenia caryophyllata on Candida albicans, Aspergillus niger and Aspergillus flavus. Biomedical and Pharmacology Journal. 2015 Jan 20;1(1):43-6.

31. Das S, Sharma S, Kar S, Sahu SK, Samal B, Mallick A. Is inclusion of Sabouraud dextrose agar essential for the laboratory diagnosis of fungal keratitis?. Indian journal of ophthalmology. 2010 Jul 1;58(4):281-5.

32. Cheng C, Liu S, Mueller BJ, Yan Z. A generic static headspace gas chromatography method for determination of residual solvents in drug substance. Journal of Chromatography A. 2010 Oct 8;1217(41):6413-21.

33. Ericsson BH, Tunevall G, Wickman K. The paper disc method for determination of bacterial sensitivity to antibiotics: relationship between the diameter of the zone of inhibition and the minimum inhibitory concentration. Scandinavian journal of clinical and laboratory investigation. 1960 Jan 1;12(4):414-22.

34. Koo J, Chou CC. PDF to PDF/A: evaluation of converter software for implementation in digital repository workflow. New Review of Information Networking. 2013 May 1;18(1):1-5.

35. Chen Y, Zhu F, Lee J. Data quality evaluation and improvement for prognostic modeling using visual assessment based data partitioning method. Computers in industry. 2013 Apr 1;64(3):214-25.

36. Azzam KA. SwissADME and pkCSM webservers predictors: An integrated online platform for accurate and comprehensive predictions for in silico ADME/T properties of artemisinin and its derivatives. Kompleksnoe Ispolzovanie Mineralnogo Syra= Complex use of mineral resources. 2023;325(2):14-21.

37. Ren Y, Kinghorn AD. Development of potential antitumor agents from the scaffolds of plant-derived terpenoid lactones. Journal of medicinal chemistry. 2020 Dec 8;63(24):15410-48.

38. Di Muzio E, Toti D, Polticelli F. DockingApp: a user friendly interface for facilitated docking simulations with AutoDock Vina. Journal of Computer-Aided Molecular Design. 2017 Feb;31(2):213-8.

39. Costa AS, Martins JP, de Melo EB. SMILES-based 2D-QSAR and similarity search for identification of potential new scaffolds for development of SARS-CoV-2 MPRO inhibitors. Structural Chemistry. 2022 Oct;33(5):1691-706.

40. Forli S, Huey R, Pique ME, Sanner MF, Goodsell DS, Olson AJ. Computational protein–ligand docking and virtual drug screening with the AutoDock suite. Nature protocols. 2016 May;11(5):905-19.

41. Baroroh U, Biotek M, Muscifa ZS, Destiarani W, Rohmatullah FG, Yusuf M. Molecular interaction analysis and visualization of protein-ligand docking using Biovia Discovery Studio Visualizer. Indonesian Journal of Computational Biology (IJCB). 2023 Jul 21;2(1):22-30.